Self-consistent electron acceleration due to inertial Alfvén wave pulses

C. E. J. Watt, R. Rankin, and I. J. Rae
Department of Physics, University of Alberta, Edmonton, Alberta, Canada

D. M. Wright
Radio and Space Plasma Physics Group, University of Leicester, Leicester, UK

Received 1 November 2004; revised 29 June 2005; accepted 7 July 2005; published 23 September 2005.

[1] We present self-consistent kinetic simulations of the electron response to finite duration shear Alfvén wave pulses in a magnetized plasma. In Earth's magnetosphere, the evidence suggests that parallel electric fields in inertial scale shear Alfvén waves can accelerate electrons in the geomagnetic field-aligned direction. Here, we study large-amplitude wave forms as they travel through ambient plasma at phase velocities which are consistent with resonant electron acceleration predicted by linear kinetic theory. Our self-consistent simulations reveal that the wave potential evolves nonlinearly as shear Alfvén wave pulses travel through the simulation domain. The evolution of the wave pulse from a symmetrical to a nonsymmetrical potential structure, and the large perturbation in the distribution function required to carry the parallel current of the pulse, leads to nonresonant acceleration of electrons (i.e., acceleration of electrons which are not traveling at the same velocity as the wave). We compare the signature of resonant and nonresonant electron acceleration with data from a low-altitude spacecraft and suggest an explanation for features often referred to as field-aligned suprathermal electron bursts. Finally, we discuss how resonant and nonresonant acceleration of electrons is affected by the perpendicular wavelength and amplitude of shear Alfvén wave pulses.

Citation: Watt, C. E. J., R. Rankin, I. J. Rae, and D. M. Wright (2005), Self-consistent electron acceleration due to inertial Alfvén wave pulses, *J. Geophys. Res.*, *110*, A10S07, doi:10.1029/2004JA010877.

1. Introduction

[2] Field-aligned electron acceleration is a key process in the generation of aurora. In particular, in situ measurements of electron energy spectra on field lines which map to the auroral oval indicate the presence of energetic electrons that have a variety of spatial and temporal characteristics. For example, the inverted-V signature that is characteristic of large-scale auroral arcs (100s of km) is a spatial structure that is generated by a significant potential drop along auroral field lines [*Evans*, 1974]. At smaller scales, there has been much recent interest in modeling electron energization by propagating shear Alfvén waves with perpendicular scale lengths that can support the generation of parallel electric fields [*Hui and Seyler*, 1992; *Kletzing*, 1994; *Thompson and Lysak*, 1996; *Chaston et al.*, 2000, 2002, 2003a, 2003b; *Kletzing and Hu*, 2001; *Su et al.*, 2004; *Watt et al.*, 2004; *Damiano and Wright*, 2005].

[3] In this paper, we focus on electron acceleration processes which vary much more quickly in time than the large scale inverted-V signature. They are associated with wave activity rather than quasi-static potential drops. In situ observations by rockets and low-altitude spacecraft show Alfvénic perturbations that are accompanied by enhancements in the electron energy flux [e.g., *Boehm et al.*, 1990]. On some occasions, these enhancements take the form of field-aligned beams of time-dispersed energetic electrons [*Kletzing and Torbert*, 1994; *Clemmons et al.*, 1994; *Arnoldy et al.*, 1999; *Ivchenko et al.*, 1999; *Lynch et al.*, 1999; *Khoyaintsev et al.*, 2000; *Yamauchi et al.*, 2001; *Andersson et al.*, 2002; *Chaston et al.*, 2002; *Su et al.*, 2004] with an associated timescale $\sim$1 s. Pitch-angle dispersion is also occasionally observed in association with these electron beams [e.g., *Kletzing and Torbert*, 1994; *Arnoldy et al.*, 1999; *Andersson et al.*, 2002]. In some cases, observations show field-aligned electron bursts which take the form of a simultaneous enhancement of differential electron energy flux at all energies below a cutoff that is typically several hundreds of eV [*Gary et al.*, 1998; *Wahlund et al.*, 1998; *Su et al.*, 2001; *Andersson et al.*, 2002; *Chaston et al.*, 2003a, 2003b; *Mende et al.*, 2003; *Su et al.*, 2004]. These bursts are sometimes referred to as suprathermal electron bursts and are usually highly field-aligned. Finally, there are also occasions where clear examples of both dispersed beam signatures and low-energy bursts are observed within the same high-resolution data set [e.g., *Andersson et al.*, 2002; *Su et al.*, 2004], and so it is possible that both signatures are due to acceleration of electrons by shear Alfvén waves with short perpendicular scale lengths.

0148-0227/05/2004JA010877

[4] If Alfvén waves are responsible for field-aligned energization of electrons, then there must be an associated wave parallel electric field. It is known that Alfvén waves carry a parallel electric field at short perpendicular wave scales comparable to either the electron skin depth $\delta_e = c/\omega_{pe}$ [*Goertz and Boswell*, 1979] or the ion acoustic gyroradius $\rho_{ia} = C_s/\Omega_i$ [*Hasegawa*, 1976], where $\omega_{pe} = (n_e q_e^2/(m_e e_0))^{1/2}$ is the electron plasma frequency, $C_s = (2k_B T_e/m_i)^{1/2}$ is the ion (proton) acoustic speed and $\Omega_i = q_i B_0/m_i$ is the ion (proton) gyrofrequency (in this paper, n_α is the number density, q_α is the charge, m_α is the mass, and T_α is the temperature of species $\alpha = \{e, i\}$). Work by *Lysak and Carlson* [1981] showed that for altitudes less than 4–5 R_E, the inertial limit is more appropriate.

[5] In order to study the electron response to propagating inertial Alfvén disturbances, we have developed a one-dimensional gyroaveraged kinetic simulation code [*Watt et al.*, 2004]. Pulses in the scalar potential ϕ are introduced at an upper boundary and allowed to propagate along the ambient magnetic field, interacting with the plasma as they travel. *Watt et al.* [2004] reported that for cases when the pulse amplitude is such that $q_e\phi \gg k_B T_e$, the nonlinear evolution of the distribution function leads to steepening of the pulse shape. In agreement with linear studies by *Kletzing et al.* [1994], the nonlinear simulations reported by *Watt et al.* [2004] demonstrate that for electrons satisfying $v < v_{ph}$, where v_{ph} is the phase velocity of the wave, a resonant interaction between electrons and shear Alfvén waves is possible due to the strong perturbation of the electron distribution function f_e produced by shear Alfvén waves. *Watt et al.* [2004] also showed that ambient plasma is heated after a pulse with $q_e\phi \gg k_B T_e$ has passed through it.

[6] In the present paper, we use kinetic simulations and test-particle diagnostics to demonstrate the underlying physics of this nonresonant energization. The test-particle analysis leads us to propose a simple self-consistent explanation for the electron signature of dispersed electrons that are followed by a thermal electron "burst"[*Yamauchi et al.*, 2001; *Andersson et al.*, 2002; *Su et al.*, 2004]. We quantify how the resonant and nonresonant acceleration of electrons is affected by changing the perpendicular scale size of the pulse and the pulse amplitude.

[7] The paper is organized in the following way. In section 2, we present data obtained from the Fast Auroral Snapshot spacecraft (FAST) [*Carlson et al.*, 1998] as a motivation for our study. Section 3 describes our kinetic simulation model, including a discussion of the assumptions used in the computer code and its validity. In section 4 we compare the data interval presented in section 2 with our simulation results and show results from a test-particle analysis as an aid to explaining the different acceleration mechanisms associated with shear Alfvén wave pulse dynamics. Section 5 presents simulation results showing the response of electrons to changing pulse amplitude and perpendicular wave number. Finally, we present the conclusions of this study in section 6.

2. Observations

[8] As motivation for our study, we present a FAST observation that shows evidence of the electron signatures mentioned in section 1. FAST is a low-altitude spacecraft that samples the dynamics of the auroral zone at very high time resolution. It was launched into an elliptical orbit with an apogee of 4175 km, perigee of 350 km, and inclination of 83°. In addition to measuring electric and magnetic fields, FAST also makes high time-resolution measurements of the energy distribution and particle fluxes associated with the auroral oval. Figure 1 shows data from the interval first discussed by *Su et al.* [2004], who proposed an explanation of the electron signatures in the data in terms of Alfvén waves. In section 6, we will compare the self-consistent results from our model with the test-particle results of *Su et al.* [2004]. We choose the same observation as it is a clear example of both the velocity-dispersed beam signature and the suprathermal electron burst signature.

[9] We utilize data from the FAST electron electrostatic analyzer (EESA) in this study, which is capable of providing raw data with full (360°) pitch angle resolution in 32 bins every 70 ms, with high energy resolution. When the spacecraft is in the auroral zone, the EESA field-of-view lies in the spacecraft spin plane and is typically aligned within 6° of the geomagnetic field. The energy range of the EESA is 4 eV to 30 keV. The magnetic field measurements are taken from the FAST Fluxgate Magnetometer (FGM), which is capable of measuring up to ±60,000 nT at a resolution of ±1 nT. In the data interval considered, the measurements were taken at ~80 ms resolution while the electric field sensors provide measurements at 5 ms resolution.

[10] From top to bottom, Figure 1 shows the downgoing differential electron energy flux (from 30 eV to 3000 eV) (Figure 1a), the electric field along the spacecraft track ($\sim E_\perp$) (Figure 1b), the electric field near the ambient magnetic field (Figure 1c), and the perpendicular magnetic field perturbation ($\sim \delta B_\perp$) (Figure 1d) from 0833:24 to 0833:30 UT on 17 July 1997 (orbit 3568). During this time interval, FAST was flying through the dayside magnetosphere (~0900 MLT) at ~3200 km altitude. The downgoing differential energy flux is calculated from those electrons heading toward the ionosphere between ±30° of the ambient magnetic field. Since our model is one-dimensional, we consider only downgoing electrons in our comparison, and therefore it is sufficient to isolate the electron flux measurements close to the field-aligned direction, rather than the full electron energy/pitch-angle information as shown in the work of *Su et al.* [2004].

[11] Concentrating first on the signatures seen in the differential electron energy flux, we can see in Figure 1a an energy dispersed signature between 0833:26.5 UT and 0833:27.1 UT. The average energy of the electrons arriving at the start of this feature is ~600 eV and this decreases to ~450 eV at 0833:27 UT. This represents an example of the velocity-dispersed signature discussed in the introduction. After 0833:27.1 UT, the energy flux is enhanced for all energies below ~300 eV which is indicative of a suprathermal electron burst. As seen in other studies [*Yamauchi et al.*, 2001; *Andersson et al.*, 2002], the velocity-dispersed signature is often immediately followed by a suprathermal electron burst signature in the electron flux data.

[12] At the time the suprathermal electron burst signature is seen in the electrons, we also see a large negative bay in E_{alongV}, which peaks at $E_{alongV} \sim -170$ mV/m. This is accompanied by two positive deviations in E_{nearB}, the first

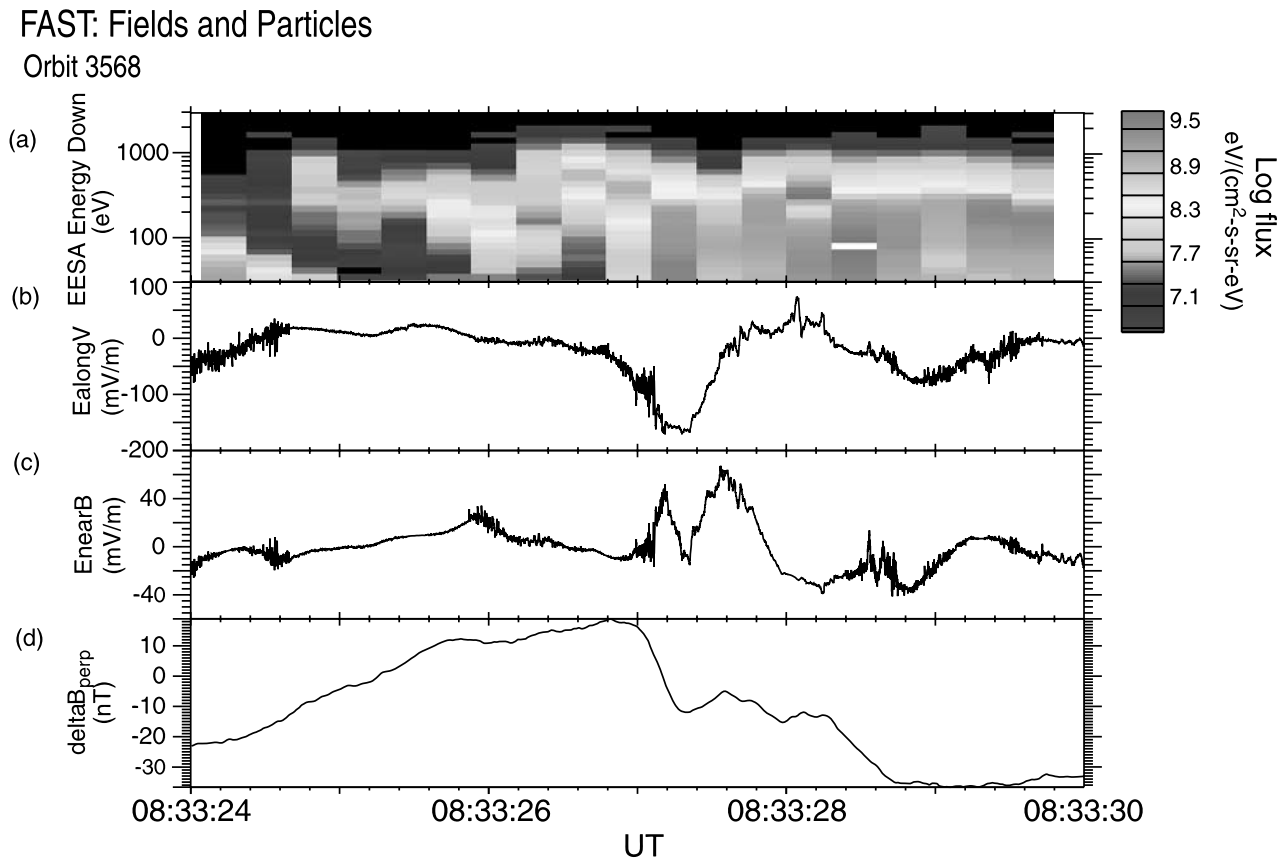

Figure 1. FAST particle and field data from 0833:24UT to 0833:30 UT 17 July 1997 (orbit 3568): (a) Downgoing differential electron energy flux (where electrons are integrated over ±30° from ambient magnetic field direction); (b) Electric field measured along the spacecraft orbit ($E_\perp$); (c) Electric field measured close to the ambient magnetic field direction; (d) Magnetic field measured perpendicular to the ambient magnetic field ($\delta B_\perp$). See color version of this figure at back of this issue.

of which peaks at $E_{nearB} \sim 50$ mV/m and the second at $E_{nearB} \sim 75$ mV/m. There is also a negative excursion through ~25 nT in $\delta B_\perp$ beginning at 0833:27 UT and ending at 0833:27.3 UT. These electromagnetic perturbations form an isolated disturbance and do not appear to be part of a periodic wave structure. *Su et al.* [2004] conclude that this pulse signature is likely to be Alfvénic since the ratio of $E_{alongV}/\delta B_\perp$ is of the same order as the local Alfvén speed. There are no significant perturbations in the electric or magnetic fields to accompany the velocity-dispersed signature. The pulse is coincident only with the suprathermal electron burst electron flux signature.

[13] In this study we concentrate on the enhancements in electron energy flux immediately before and during the pulse in the electromagnetic fields. It is interesting to note that there is a less intense energy-dispersed signature between 0833:25.2UT and 0833:26.2 UT, which is possibly associated with a small disturbance in E_{nearB} (~25 mV/m) but which does not occur prior to a large δB or E_{alongV} perturbation. We also note that the duration of the pulse in the FAST data set is ~0.5 s, and the spacecraft is traveling across the ambient magnetic field with a velocity of ~6 km/s. If the electron signatures are due to a shear Alfvén wave with perpendicular scale length comparable to the local electron skin depth ($\delta_e \sim 1$ km) then the measurements will exhibit a mixture of both spatial and temporal structure as the pulse passes over the spacecraft. It is important to point out that the simulation being used in this paper is one-dimensional. Investigations of spatial structure perpendicular to the magnetic field is left for future study.

3. Model Equations and Simulation Domain

[14] We present results from a one-dimensional self-consistent gyroaveraged Vlasov kinetic code [*Watt et al.*, 2004] which follows three quantities in time: the electron distribution function f_e, the parallel component of the vector potential $A_\parallel$, and the scalar potential ϕ. In order to limit the dimensions required in our simulation code, we assume that fields vary across the ambient magnetic field as exp $(-ik_\perp x)$, where $k_\perp$ is the perpendicular wave number and x is a perpendicular coordinate. This means that the perpendicular wave number for each simulation must be specified at the outset, and the perpendicular dynamics cannot change during the course of the simulation. In future work, we hope to compare our code results with particle-in-cell simulations or hybrid simulations of higher dimensionality, in order to identify the accuracy of our one-dimensional simulation results.

[15] Most kinetic simulation models of mesoscale physics (scale lengths much larger than the electron debye length,

λ_{De}) make use of assumptions that are necessary to isolate and render tractable the most important physics. Although it is an idealization, all of the simulation results detailed in this paper involve a uniform ambient magnetic field. Future investigations involving our model will include nonuniformity in the magnetic field, number density, and temperature profile, in order to study the effect of the mirror force and the varying Alfvén speed and electron skin depth along the field line. Even with our simplifying assumptions, we retain vital nonlinear physics in our model. The wave potentials are allowed to evolve self-consistently according to the response of the plasma to the waves, and our results show that the nonlinear electron dynamics in this process is critical.

[16] In the derivation of the governing equations, we have assumed that the displacement current term in Ampére's Law is negligible. While this assumption is valid in most parts of Earth's magnetosphere, it may be necessary to revise this assumption when dealing with plasmas with deep density cavities or indeed when dealing with other planetary magnetospheres where the Alfvén speed is very high (e.g., Jupiter).

[17] On the basis of the above assumptions, the simulation uses three governing equations:

$$\frac{\partial f}{\partial t} + \left(p_\parallel - \frac{q_e}{m_e}A_\parallel\right)\frac{\partial f}{\partial z} + \left[\frac{q_e}{m_e}\left\{\left(p_\parallel - \frac{q_e}{m_e}A_\parallel\right)\frac{\partial A_\parallel}{\partial z} - \frac{\partial \phi}{\partial z}\right\} - \frac{\mu}{m_e}\frac{\partial B_0}{\partial z}\right]\frac{\partial f}{\partial p_\parallel} = 0, \tag{1}$$

$$A_\parallel = \frac{\mu_0 q_e \int_{-\infty}^{\infty} p_\parallel f dp_\parallel}{k_\perp^2 + \mu_0 \frac{q_e^2}{m_e}\int_{-\infty}^{\infty} f dp_\parallel}, \tag{2}$$

$$\frac{\partial \phi}{\partial t} = -v_A^2 \frac{\partial A_\parallel}{\partial z}. \tag{3}$$

The wave potentials in the above set of equations are discretized on fixed grids in the spatial coordinate z, and the distribution function is discretized on a fixed grid in phase space, with parallel momentum coordinate $p_\parallel = v_\parallel + (q_e/m_e)A_\parallel$ and spatial coordinate z. The spatial coordinate represents distance along a magnetic field line with $z = 0$ representing the lower end of the simulation domain in altitude and $z = L_z$ representing the upper end. The model equations and algorithm are discussed in detail in the work of *Watt et al.* [2004]. For a simulation with uniform magnetic field, the final term in the square brackets in equation (1) (the mirror force term) is zero.

[18] The boundary conditions for the potentials are as derived by *Lysak* [1991] and reflect the physical properties desired at each boundary. The lower boundary represents a conducting layer which can be characterized by a uniform height-integrated Pedersen conductivity:

$$A_\parallel(z = 0) = -\mu_0 \Sigma_p \phi(z = 0). \tag{4}$$

The upper boundary condition on the potential allows upward propagating waves to leave the simulation domain and minimizes reflection:

$$\phi(z = L_z) = \phi_0(t) + v_A A_\parallel. \tag{5}$$

At each end of the simulation domain, the plasma entering the domain is assumed to be of Maxwellian form with a fixed number density n_e and temperature T_e. For these uniform simulation runs, the incoming n_e and T_e are set to the initial simulation values. The electron drift velocity v_{de} is constrained to be consistent with the parallel current required to support the $A_\parallel$ at $z = 0$ and $z = L_z$. These boundary conditions have been rigorously tested to ensure that they do not introduce numerical errors into the results.

[19] The simulation is initiated with constant uniform values of temperature and number density, and the initial electron drift velocity is zero, i.e., $f_e(v, t = 0)$ is initially identical at all spatial grid points. The potentials are perturbed at the top of the simulation domain, and the resulting disturbance propagates through the simulation domain, which corresponds to a plasma of length $L_z = 4.7$ R_E with spatial grid resolution $\Delta z = 0.005$ R_E. The number of $p_\parallel$-grid points varies with the physical input parameters for each simulation. In each case, the grid has sufficient range to ensure that values of f_e at the grid boundary are small and that the bulk of the distribution function is adequately resolved. To achieve this, we employ a nonuniform $p_\parallel$-grid which is the same at each spatial grid point. The $p_\parallel$-grid points are closely spaced for $p_\parallel < v_{th}$ (where $v_{th} = (2k_B T_e/m_e)^{1/2}$ is the electron thermal speed) and the spacing between grid points gets larger as $|p_\parallel|$ increases. The initial pulse amplitude ϕ_0 is used to estimate an upper bound for values of $A_\parallel$ in the simulation. The maximum value of $p_\parallel$ is then set at $p_{\max} = 8v_{th} + (q_e/m_e)A_{\max}$, and the minimum value of $p_\parallel$ is set equal to $-p_{\max}$. The smallest $p_\parallel$-grid spacing is $0.1v_{th}$ at $p_\parallel \sim 0$, and then the grid spacing increases for increasing $p_\parallel$ according to a geometrical progression. Typically, the number of $p_\parallel$-grid points is $200 < N_p < 400$. We have performed simulations with varying grid resolution and have established that the effects we see are due to physical processes and not numerical artifacts.

4. Comparison Between Observations and Modeling

4.1. Simulation Results

[20] Our simulations of Alfvén wave pulses with $\lambda_\perp \sim \delta_e$ show differential electron flux signatures similar to Figure 1. In what follows, we use these simulation results to guide our interpretation of FAST electron signatures.

[21] In order to present the simulation data in a way that most closely approximates the satellite data, we choose a point along the simulation domain and plot the simulation parameters as a function of time. As previously mentioned, we are unable to study perpendicular spatial variation with our one-dimensional code. We also note that the FAST spacecraft is likely to be moving significantly across the wave structure as the pulse passes over it due to the short perpendicular scale lengths involved. Nonetheless, keeping these caveats in mind, it is instructive to compare the

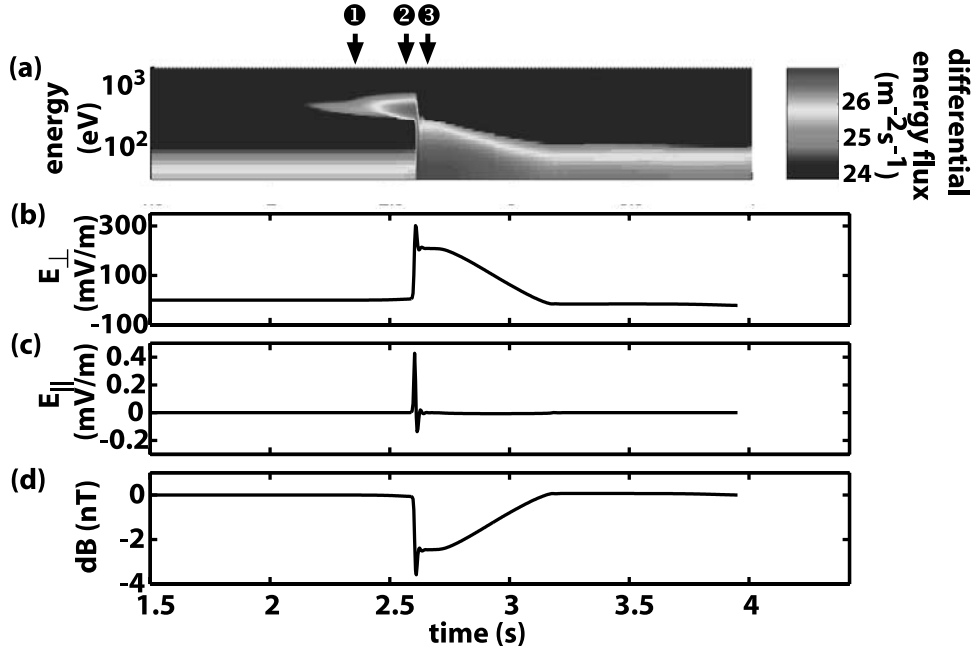

Figure 2. Simulation parameters calculated at $z = 1\ R_E$ from the lower boundary of the simulation as a function of time: (a) Differential energy flux of downgoing electrons; (b) Perpendicular electric field; (c) Parallel electric field; (d) Perpendicular magnetic field. Times marked 1, 2, and 3 are used in Figure 3. See color version of this figure at back of this issue.

simulation results with the spacecraft observations shown in Figure 1.

[22] We first of all study the results of a uniform magnetic field simulation with the following input parameters: $n_e = 1.7 \times 10^8$ m^{-3}, $k_B T_e = 10.0$ eV, $B_0 = 17{,}000$ nT, and $k_\perp = 8.0 \times 10^{-3}$ m^{-1}, which corresponds to $\delta_e k_\perp = 3.3$. The number density and magnetic field are chosen to represent typical values at the FAST altitude height (~3200 km) while the perpendicular scale length ensures that a parallel electric field forms in the shear Alfvén wave.

[23] A Gaussian-shaped pulse is added to the scalar potential at $z = L_z$ which propagates down the simulation domain. The initial amplitude of the pulse at $z = L_z$ is $\phi_0 = 40$ V ($E_\perp = 320$ mV/m) and the duration of the initial pulse is 0.5 s ($\gg 2\pi/\Omega_i$). Note that since $q_e\phi > k_B T_e$, the pulse steepens as it propagates [see *Watt et al.*, 2004] and the parallel electric field, which is originally bipolar and symmetric, evolves into an asymmetric shape which will be discussed in detail elsewhere in this paper.

[24] Figure 2 shows the time evolution of the simulation parameters at a distance $z = 1\ R_E$ from the lower end of the simulation box: the downward differential energy flux, $|m_e v_\parallel^3 f_e(v_\parallel)|$, for f_e with $v_\parallel < 0$ (downward is the negative direction in the simulation) (Figure 2a); perpendicular electric field $E_\perp = -(\nabla.\ \phi)_\perp = -k_\perp \phi$ (Figure 2b); the parallel electric field $E_\parallel = -(\partial\phi/\partial z) - (\partial A_\parallel/\partial t)$ (Figure 2c); and the perpendicular magnetic field $\delta B = (\nabla \times A_\parallel)_\perp = -k_\perp A_\parallel$ (Figure 2d). The units used in this plot are the same as in Figure 1. Note that the pulse has traveled through 3.7 R_E of uniform plasma before reaching the point $z = 1\ R_E$. We see in Figure 2 a velocity-dispersed beam signature during the interval $2.10 < t < 2.60$ s. The electrons which arrive during the interval $2.10 < t < 2.30$ s were accelerated at the top of the simulation domain before the wave evolved into the steepened shape seen in Figures 2b and 2d. Hence they have lower energies than electrons which arrive during the interval $2.30 < t < 2.60$ s to form a velocity-dispersed signature. The average energy of the beam electrons during the interval $2.30 < t < 2.60$ s falls from ~600 eV to ~400 eV at $t = 2.60$ s.

[25] Note that the simulation results presented here are for a uniform magnetic field and so there will be no velocity dispersion seen at the highest beam energies. Electrons undergo resonant acceleration all the way along the simulation domain and so the highest-energy electrons will always be present in the beam signature. Also, it is important to note that in a simulation with uniform magnetic field and number density, the duration of the beam signature at this position in the simulation domain will depend only upon the amount of plasma the pulse has traveled through before reaching this point, i.e., the length of the simulation domain. In simulations of longer length, such that there is a larger distance between $z = 1\ R_E$ and the top of the simulation domain, the beam signature has a longer duration but has the same characteristic energies.

[26] The burst signature seen in the Figure 2 simulation results, during the interval $2.60 < t < 3.10$ s, shows an enhancement of downward electron energy flux at all energies <300 eV. This energy flux enhancement is associated with discrete electric and magnetic field signatures. Coincident with the start of the enhancement of the energy flux at $t = 2.60$ s, $E_\perp$ starts to increase to a peak of $E_\perp \sim 300$ mV/m at $t = 2.62$ s. During the large $E_\perp$ perturbation, $E_\parallel$ first exhibits an antisymmetric bipolar signature which peaks at $E_\parallel = 0.4$ mV/m, and is followed by a period of small, negative $E_\parallel$ for the interval $2.70 < t < 3.10$ s. The

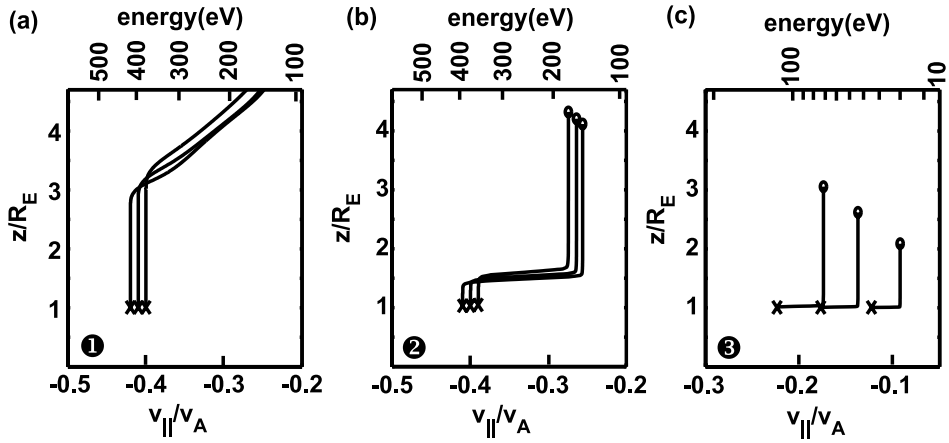

Figure 3. Trajectories of particles traced backward through the simulation fields from an original position of $z = 1\ R_E$: (a) Beam particles traced backward from $t_1 = 2.30$ s; (b) Beam particles traced backward from $t_2 = 2.55$ s; (c) Burst particles traced backward from $t_3 = 2.61$ s.

perpendicular magnetic field deviation also starts at $t = 2.60$ s and lasts for the same amount of time as the deviation in $E_\perp$. The peak deviation corresponds to $\delta B = -3.5$ nT.

[27] If we compare the simulation results discussed above to the data interval presented in Figure 1, we can see some clear similarities. The velocity dispersed signature in each case arrives before the pulse, and the simulation velocity-dispersed signature shows a similar energy range to that seen in Figure 1. In both the spacecraft data and simulation data, there is a large increase in electron energy flux for all energies <300 eV during the burst signature. The spacecraft data shows that the burst signature is accompanied by a large amplitude negative bay in E_{alongV}, whereas the simulation shows a large amplitude positive perturbation during the energy flux enhancement. Note that although the sign of the pulse in the simulation $E_\perp$ is opposite to the sign of E_{alongV} in the spacecraft data, the magnitudes of the pulses are of the same order. However, the magnitude of the change in δB is much less in the simulation data than in the spacecraft data. We remind the reader that the simulations used in this paper are for uniform magnetic fields and this may explain this disparity. In particular, the spacecraft data shows signatures of an Alfvénic pulse which has traveled along a field line of increasing magnetic field strength. This will change the amplitude of the pulse as it propagates. We will investigate this effect in future simulations which will include a nonuniform magnetic field.

4.2. Location and Timing of Acceleration Events

[28] As mentioned in section 1, test particles can be used to investigate the motion through phase space of different elements of the distribution function derived from the Vlasov simulation code. In this manner, we can determine the origin of the accelerated electrons for each signature in the electron energy flux.

[29] We shall use Figure 2a to identify groups of accelerated electrons that we wish to trace through the simulation. We choose high-energy electrons at time $t_1 = 2.30$ s (indicated by a "1" at the top of Figure 2a) which are among the first accelerated electrons to arrive at the point $z = 1\ R_E$ long before the arrival of the pulse. We also choose high-energy beam electrons at time $t_2 = 2.55$ s, which is immediately prior to the pulse's arrival at $z = 1\ R_E$ (indicated by a "2" at the top of Figure 2a). As well as the high-energy beam electrons, we are interested in tracing the history of those particles which form the burst signature and so we choose some lower-energy particles at time $t_3 = 2.61$ s (indicated by a "3" at the top of Figure 2a).

[30] Figure 3 shows the time histories of test particles which have been moved through the simulation domain using the parallel electric field obtained from the simulation. We use the following equations to follow their progress:

$$\frac{\partial z}{\partial t} = v_z \tag{6}$$

$$\frac{\partial v_z}{\partial t} = \frac{q_e}{m_e} E_\parallel(z,t). \tag{7}$$

Electrons are traced backward in time from times t_1 (Figure 3a), t_2 (Figure 3b), and t_3 (Figure 3c). Each line represents the trajectory of a particle, with a circle to show the original position and velocity of the particle (at $t = 0$) and a cross to show its final position and velocity (at $t = t_1$, t_2, t_3). There are no circles in Figure 3a because the particles originate at the very top boundary of the simulation. The vertical axis gives the spatial location z, and since these are all downward moving electrons, we can follow each electron's progress in time by following its trajectory from the top to the bottom of the plot. The lower horizontal axis shows the electron speed normalized to the ambient Alfvén velocity $v_A = B_0(\mu_0 m_i n_i)^{-1/2}$, and the upper horizontal axis shows the corresponding energy values.

[31] The location at which each electron is accelerated can be determined from where they move in a horizontal direction in the phase-space plots. If we concentrate first on the beam electrons, Figure 3a shows that those beam electrons which arrive at $z = 1\ R_E$ first (at $t = t_1$) are accelerated at the very top of the simulation domain. On the other hand, Figure 3b shows that the beam electrons, which arrive at $z = 1\ R_E$ immediately prior to the pulse, are accelerated at $z = 1.5\ R_E$, a point much closer to the observation location. Note that the electrons are accelerated

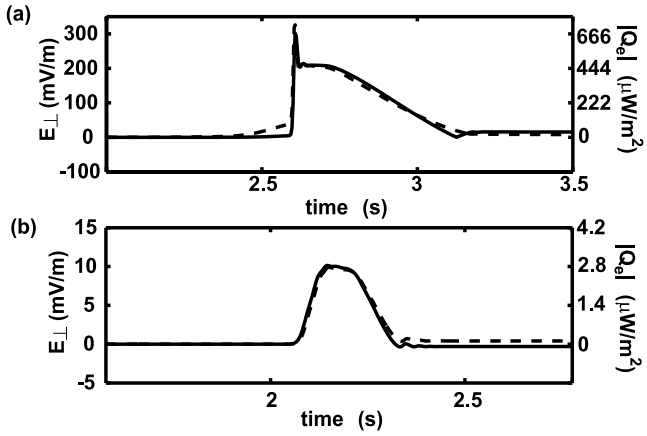

Figure 4. Evolution of perpendicular electric field $E_\perp$ (solid lines) and the magnitude of total electron energy flux $|Q_e|$ (dashed lines) for (a) the simulation run shown in Figure 2 (ϕ_0 = 40 V) and (b) a similar simulation run with smaller initial pulse amplitude (ϕ_0 = 2 V).

over a much shorter spatial distance at $z = 1.5\ R_E$ than at $z = 4.7\ R_E$. This also indicates the evolution of the wave pulse shape as it travels down the simulation domain. Figure 3c reveals a clear difference in the acceleration location of those electrons which form the suprathermal electron burst signature, from those which are in the beam. The burst electrons are accelerated locally, at almost exactly the same location as they are observed. If we follow the trajectory of the electrons in Figure 3c after $t = 2.61$ s (not shown), they are also decelerated locally and have not traveled far in the process (distance traveled while accelerated <0.5 R_E).

[32] Although Figure 3c shows the location of the electron energization to form the suprathermal electron burst, it does not yield any information regarding the timing of the energization with respect to the arrival of the pulse at $z = 1\ R_E$. The total parallel energy flux Q_e is a useful indicator of the acceleration of electrons, and so we compare it with the magnitude of $E_\perp$ in order to investigate the relative timing between pulse arrival and suprathermal electron burst energization. From studying many different simulation runs with different initial parameters, it is clear that Q_e evolves differently when a beam is formed than when there is insufficient resonant acceleration to form a beam. We show both cases in Figure 4. The evolution of $|Q_e|$ (dashed line) and $|E_\perp|$ (solid line) at $z = 1\ R_E$ is shown in Figure 4a for the simulation run previously discussed in this section and in Figure 4b for an identical simulation run with a smaller pulse amplitude ϕ_0 = 2 V (where no beam is formed). In both cases, there is a very good correlation between the enhancement in $|Q_e|$ and the magnitude of $E_\perp$ during the pulse, even when the pulse exhibits significant steepening due to wave-particle interactions. Figure 4a shows that the beam can be identified as a small enhancement in $|Q_e|$ prior to the arrival of the pulse. We identify the large total electron energy flux enhancement, which is coincident with the $E_\perp$ perturbation, as the local acceleration and deceleration of the bulk distribution function.

[33] The results discussed above reveal that as previously thought, the beam electrons are precipitating electrons which originate at locations above the observation point. On the other hand, the suprathermal electron burst represents electrons that are accelerated and decelerated locally in order to carry the parallel current associated with the shear Alfvén wave pulse. These electrons will not carry wave energy to other locations and thus they cannot be considered to be accelerated in the same sense as beam electrons. Local acceleration and deceleration of electrons was also observed in linear models which included the full electron distribution function [*Kletzing*, 1994; *Kletzing and Hu*, 2001].

[34] In order to interpret electron energy signatures in auroral region satellite data, it is important to make a distinction between electrons which are locally accelerated and decelerated and precipitating electrons, i.e., those electrons which have been accelerated elsewhere and are no longer interacting with the wave. For example, *Su et al.* [2001] show that enhancements of field-aligned electron energy flux are well-correlated with small-scale variations of the perpendicular electric field. These perpendicular electric field perturbations are believed to be due to propagating Alfvén waves. The authors concluded that the bursts of electron energy flux are precipitating electrons which have been energized by the Alfvén waves. In a similar vein, other authors speak of electrons forming a suprathermal electron burst as "arriving together with the wave" [*Yamauchi et al.*, 2001]. The simulation results presented here suggest a different interpretation of suprathermal burst signatures and reveal them to be locally accelerated electrons, not precipitating electrons which have been accelerated at another location.

4.3. Nonresonant Heating

[35] The test-particle analysis used in the previous section is a useful aid for describing the nonresonant energization of particles which persists after the pulse has passed. For times $t > 3.10$ s in Figure 2, we can see that bulk plasma has been heated by the pulse, although this energization is not as strong as the energization during the suprathermal electron burst. The effective temperature of the plasma can be calculated from the simulation as follows:

$$k_B T_{eff} = m_e \left[\left(\frac{1}{n_e} \right) \int_{-p_{\max}}^{p_{\max}} v_\parallel^2 f_e dv_\parallel - \left(\frac{1}{n_e} \int_{-p_{\max}}^{p_{\max}} v_\parallel f_e dv_\parallel \right)^2 \right], \quad (8)$$

where $n_e = \int_{-p_{\max}}^{p_{\max}} f_e dv_\parallel$. The temperature of the plasma at the beginning of the simulation is $k_B T_e$ = 10 eV (initial plasma distribution function is Maxwellian). After the pulse passes, the effective temperature of the plasma is $k_B T_{eff}$ = 12.5 eV, and it remains at this temperature until the reflected pulse travels back up the field line from the lower boundary. This nonresonant energization is due to the nonsymmetrical nature of the parallel electric field associated with the pulse.

[36] We can use test particle tracing to show the effects of the nonsymmetrical $E_\parallel$ field which develops in the simulations. Figure 5 shows the trajectories of test particles which have been traced backward from $z = 2\ R_E$ at $t = 2.60$ s, long after the pulse has passed over that position. Figure 5 shows downward (Figure 5a) and upward (Figure 5b) moving electron trajectories, respectively, with identical axes and plotting symbols to those used in Figure 3. Particles are chosen such that they have

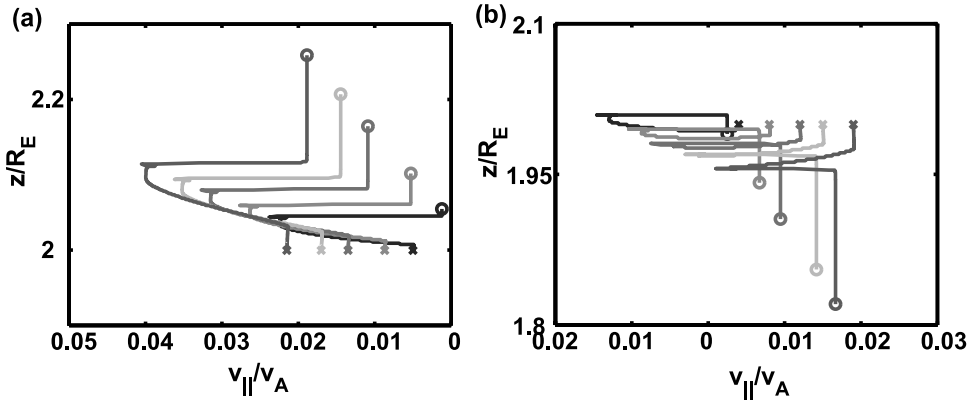

Figure 5. Trajectories of particles traced backward through the simulation fields from an original position of $z = 2\ R_E$ at $t = 2.6$ s: (a) downgoing and (b) upgoing particles representing the bulk of the heated distribution function. See color version of this figure at back of this issue.

final velocities in the bulk of the heated distribution function. Analysis of many particles shows that the velocity gain by each particle is not a simple function of the original velocity of the particle. In order to understand these gains in energy, we need to study the parallel electric field that each particle "sees."

[37] As mentioned in section 4.1, in order to model pulse propagation in the simulation, we apply a Gaussian-shaped pulse in scalar potential at the top end of the simulation domain, which results in a symmetrical $E_{||}$ at the top of the simulation domain at early times in the simulation. However, for $q_e\phi \gg k_B T_e$, the pulse experiences nonlinear steepening as it propagates through the plasma [see *Watt et al.*, 2004] and the $E_{||}$ rapidly becomes asymmetric. The wave parallel electric field is self-consistently evolving throughout its journey from the top end of the simulation domain to the lower end, although the biggest changes occur near the top of the simulation domain.

[38] Both the upward and downward thermal population experience heating after the pulse has passed, and so to explain this heating we analyze the parallel electric field experienced by both an upward and a downward moving particle (which we will call particle U and particle D, respectively). Both particles have original speeds which are less than the thermal speed and therefore represent bulk distribution particles. Figures 6a and 6b show the parallel electric field experienced by particle U and particle D, respectively. Figures 6c and 6d show the resultant velocity changes for particles U and D, respectively. At first glance, the $E_{||}$ shown in Figures 6a and 6b appear similar. However, there are subtle and important differences: if we consider the particle velocities in the wave frame, then it could be argued that both particle U and particle D should experience the same wave field, since they would both be traveling at essentially v_{ph} in the wave frame (analysis of simulation results gives $v_{ph} = -1.24 \times 10^7$ m/s or $\sim 12 v_{th}$ in the downward direction). However, if we consider the velocities of particles U and D in the wave frame as they encounter the pulse, particle U is decelerated from $1.02 v_{ph}$ to $0.98 v_{ph}$ during the interval of positive $E_{||}$, whereas particle D is decelerated from $0.98 v_{ph}$ to $0.92 v_{ph}$ during its encounter with positive $E_{||}$. This difference in wave frame velocity is small but sufficient to allow particle U and particle D to experience subtly different wave fields for different lengths of time and ultimately to experience changes of momentum, as shown in the approximate calculation which follows.

[39] The changes in particle velocity when particles U and D, discussed above, encounter the positive $E_{||}$ associated with the pulse, is a result of the large perturbation in f_e required to carry the parallel current required for the shear Alfvén wave pulse. We use an impulse-momentum argument to provide an approximate calculation of the overall change in momentum of these thermal electrons. We consider two time intervals for each particle: the first is the short time interval $(\Delta t)_1$ during which the particle experiences a large amount of acceleration due to (largely) positive electric field; the second time interval $(\Delta t)_2$ is the longer time interval during which the particle experiences slow deceleration due to the small negative electric field. These intervals are indicated with dashed lines in Figure 6.

[40] For each particle, we calculate the impulse of the acceleration J^+ during $(\Delta t)_1$ by multiplying the average force $F_{ave} = \langle q_e E_{||} \rangle$ by the time interval $(\Delta t)_1$. Similarly, we can calculate the impulse of the deceleration J^- using the time interval $(\Delta t)_2$. From the impulse-momentum theorem, we obtain an expression for the estimated change in particle velocity $(\Delta v)_{est} = (J^+ + J^-)/m_e$. The actual value of the change in test-particle velocity $(\Delta v)_{sim}$ can be calculated from Figures 6c and 6d. The values of $(\Delta t)_1$, $(\Delta t)_2$, J^+, J^-, $(\Delta v)_{est}$, $(\Delta v)_{sim}$ and the error in $(\Delta v)_{est}$ can be found in Table 1. It is difficult to unambiguously define the time interval during which "acceleration occurs" since, during the initial part of the pulse, $E_{||}$ has a complicated structure. However these approximate calculations agree with the test-particle velocity changes to within a few percent.

[41] We conclude that the energization of thermal electrons traveling both up and down the field line, after the pulse has passed, is due both to the nonsymmetrical nature of $E_{||}$ and to the large perturbation in f_e that is required to support the parallel current of the large-amplitude pulse. Analysis of the smaller amplitude runs in the following section reveals that the heating behind the pulse decreases significantly as the pulse amplitude is decreased. For small pulse amplitudes, the nonlinear steepening is reduced, and the perturbation of the thermal electrons is also reduced

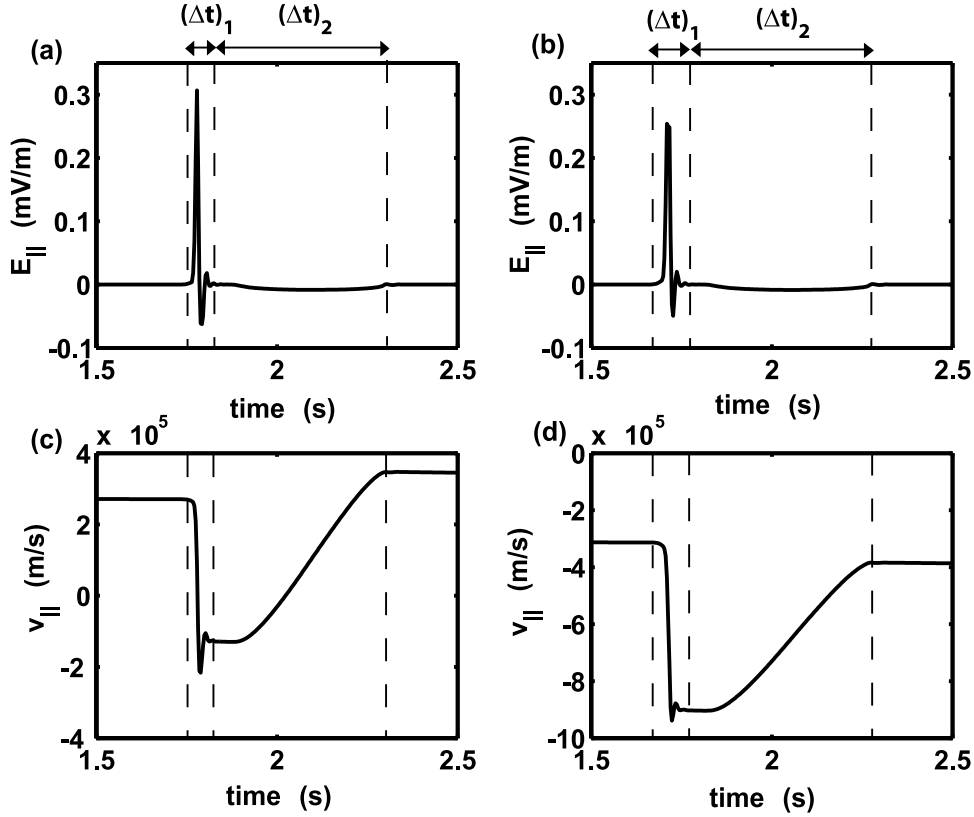

Figure 6. (a) Parallel electric field and (c) velocity experienced by an originally downward-moving thermal electron; (b) Parallel electric field and (d) velocity experienced by an originally upward moving thermal electron. Dashed lines indicate the time intervals $(\Delta t)_1$ and $(\Delta t)_2$ required for the impulse-momentum calculation.

because a lower-amplitude pulse will require a lower parallel current. Hence this nonresonant heating effect is amplitude dependent. We note that this effect cannot be observed in linear models.

5. Parameter Analysis

[42] The amount of resonant and nonresonant acceleration associated with shear Alfvén wave pulses is affected by both the amplitude of the pulse and the perpendicular scale length. In this section, we study the effects of varying these two parameters while keeping the other simulation parameters constant. For the simulation results presented in this section, we consider a one-dimensional plasma with a constant ambient magnetic field of B_0 = 6500 nT. The initial uniform number density is n_e = 1.5×10^7 m^{-3} and the initial plasma temperature is T_e = 10 eV. This yields an Alfvén speed of $v_A = 3.66 \times 10^7$ m/s. We choose these parameters to represent plasma at an altitude of 7000 km from Earth's surface following *Kletzing* [1994]. In each simulation, a Gaussian-shaped pulse of length 0.25 s is applied to ϕ at the top of the simulation domain. For the purposes of comparing each simulation run, we focus on the interaction between the pulse and the plasma before the pulse reaches the lower boundary.

[43] We first study the effects of changing the pulse amplitude by performing eight simulation runs with exactly the same initial parameters, except for the amplitude of the initial pulse ϕ_0. As before, we will look at the evolution of quantities at one spatial point in the simulation domain (z = 1 R_E) in order to directly compare the results. The perpendicular wave number for these eight runs is $k_\perp = 2.63 \times 10^{-3}$ m^{-1}, which corresponds to $k_\perp \delta_e = 3.6$ [c.f. *Kletzing*, 1994]

[44] Figure 7a shows the evolution of the total parallel electron energy flux Q_e at z = 1 R_E for each of the eight simulations. From the lowest curve to the top curve, the initial pulse amplitude is ϕ_0 = 5, 10, 20, 50, 75, 100, 150, 200 V. The curves representing $Q_e(t)$ for each run have been lagged such that the arrival of the pulse is synchronized at

Table 1. Values Calculated From Test Particle Analysis of Thermal Electrons for Use in the Impulse-Momentum Theorem to Explain Heating of Bulk Plasma After the Pulse Has Passed Through the Plasma

	Upward (U)	Downward (D)
$(\Delta t)_1$	0.1445 s	0.1617 s
$(\Delta t)_2$	0.4334 s	0.4678 s
J^+	-3.566×10^{-25} Ns	-5.2684×10^{-25} Ns
J^-	4.3066×10^{-25} Ns	4.6911×10^{-25} Ns
$(\Delta v)_{est}$	8.13×10^4 m/s	-6.34×10^4 m/s
$(\Delta v)_{sim}$	7.67×10^4 m/s	-7.11×10^4 m/s
Error	6%	11%

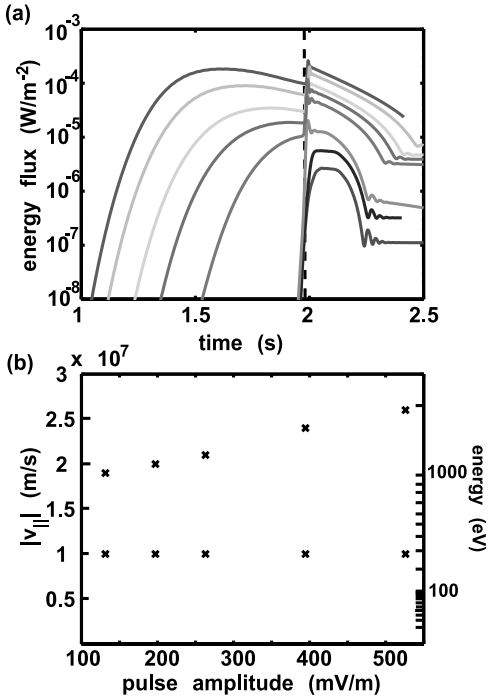

Figure 7. (a) Evolution of the total parallel electron energy flux at $z = 1\ R_E$ for eight simulation runs with identical initial parameters except for the initial pulse amplitude ϕ_0: from bottom to top ϕ_0 = 5, 10, 20, 50, 75, 100, 150, 200 V. The curves have been lagged such that the arrival of the pulse is synchronized at $t = 1.95$ s. (b) Velocity range of the resonantly accelerated electrons for those simulation runs which generated a beam (where $\phi_0 \geq 50$ V). See color version of this figure at back of this issue.

$t = 1.95$ s. In each case, for $t > 1.95$ s, the shape of the energy flux curve reflects the electron current required to support the pulse, as discussed in section 4.2. We can clearly see that an increase in initial pulse amplitude results in an increase in energy flux, which is consistent with the idea that the energy flux enhancement seen during the pulse is simply a displacement of f in the $-v$ direction in order to carry the parallel current. Note that negative velocities in the simulation correspond to downward moving particles. If there is sufficient resonant acceleration that a beam develops, then the electron energy flux will be enhanced for $t < 1.95$ s. A significant beam is only formed ahead of the pulse for the five simulations with $\phi_0 \geq 50$ V or $E_{\perp 0} \geq 130$ mV/m. As the pulse amplitude is increased, the distribution function is more strongly perturbed in the $-v_{\|}$ direction in order to carry the parallel current. Hence for $\phi \geq 50$ V, f_e is sufficiently perturbed such that enough electrons are moved into the region $v_{\|} \sim v_{ph}$ to produce a noticeable beam. A pulse amplitude of $\phi < 50$ V does not resonantly accelerate enough electrons to produce a significant acceleration signature. If the amplitude is high enough to produce an observable beam of accelerated electrons, then the energy flux contained in the beam increases with increasing pulse amplitude.

[45] Figure 7b shows the velocity range of electrons accelerated in those simulations which produced a beam. Since negative velocities correspond to downward moving particles, here we show the range of $|v_{\|}|$ as a function of amplitude. In each case, the lowest beam velocity is the same and is equal to the phase velocity of the pulse (the perpendicular scale length is the same for all simulations in this figure). The upper beam velocity increases as the amplitude of the pulse increases. *Kletzing* [1994] proposed that the energy gain of the beam electrons was due to one-interaction Fermi acceleration. Under this type of acceleration, the final velocity depends upon the size of the potential drop in the wave frame and so this mechanism can easily explain the increase in upper velocity of the beam electrons as the pulse amplitude is increased.

[46] Next, we investigate the effects of changing the perpendicular scale length of the pulse. We study six different simulation runs which each have the same initial parameters, except for the perpendicular wave number. We keep the initial pulse amplitude constant by adjusting ϕ_0

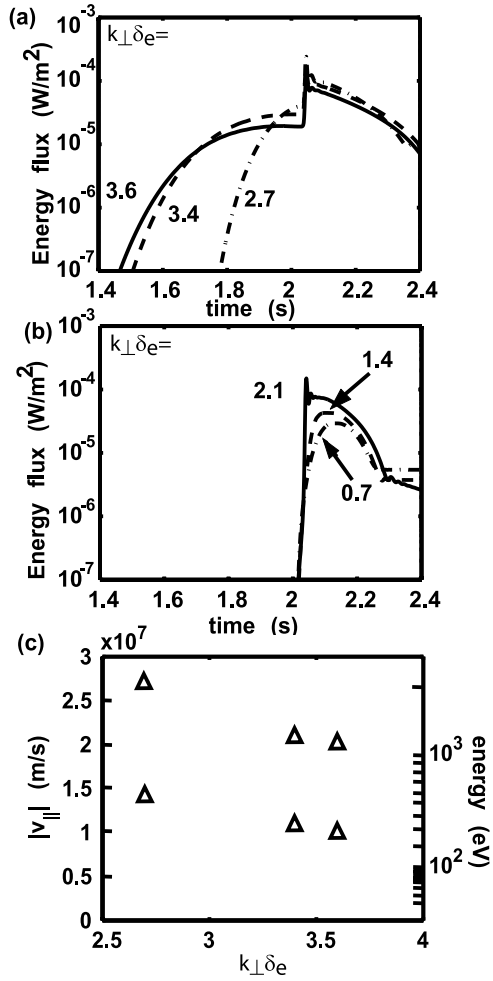

Figure 8. (a) Evolution of the total parallel electron energy flux at $z = 1\ R_E$ for six simulation runs with identical initial parameters except for the perpendicular wavelength of the pulse $k_{\perp}\delta_e = 2.7$, 3.4, and 3.6; (b) same as Figure 8a but with $k_{\perp}\delta_e = 0.7$, 1.4 and 2.7; (c) velocity range of the resonantly accelerated electrons for those simulation runs shown in Figure 8a.

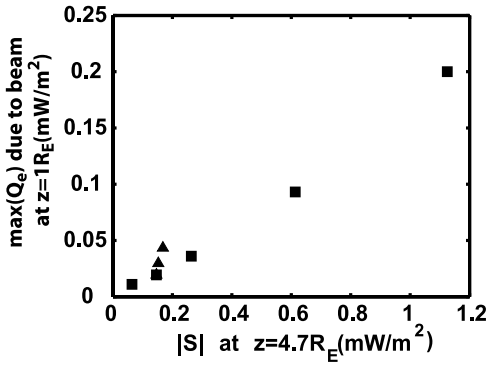

Figure 9. Maximum beam energy flux at $z = 1\ R_E$ as a function of the magnitude of the wave Poynting vector at the top of the simulation domain. Only those runs in the parameter study which produced a beam ahead of the pulse are used for this figure. Squares indicate simulation runs used in the pulse amplitude study and triangles indicate simulation runs used in the perpendicular scale length study.

such that $E_{\perp 0} = -k_\perp \phi_0$ is equal for each simulation. We only specify the amplitude of ϕ at the beginning of each simulation; the other simulation parameters, $A_\parallel$ and f_e, evolve self-consistently and hence we cannot specify exactly the magnitude of the Poynting vector for each combination of $k_\perp$ and ϕ_0. For the six runs in the $k_\perp$ study, the initial magnitude of the Poynting vector varies between 14.6 mW/m^2 and 21.4 mW/m^2.

[47] Figures 8a and 8b shows the evolution of the electron energy flux at $z = 1\ R_E$ for each of six runs, with three curves in each plot for clarity. Again, the timescale of each run has been lagged so that the arrival of the pulse is at the same time for each curve. The ratio of perpendicular wavelength is varied from $k_\perp \delta_e = 0.7$ to $k_\perp \delta_e = 3.6$. From Figure 8a we can see that for $k_\perp \delta_e \geq 2.7$ some electrons are resonantly accelerated to form a beam which arrives ahead of the pulse, whereas for those runs with $k_\perp/\delta_e \leq 2.1$, Figure 8b shows that there is no noticeable beam.

[48] Figure 8c shows the range of beam velocities for those simulation runs presented in Figure 8a. In this case, as the perpendicular wave number increases, both the lowest and highest beam velocities are decreased. Here, the lowest and highest beam velocities are controlled by the phase velocity of the wave, which increases as $k_\perp$ decreases. Figure 8a shows that for $k_\perp \delta_e = 3.4$ and 3.6, the total electron energy flux contained in the beam is roughly the same. Figure 8c shows that these parameters lead to beams with slightly different velocity ranges, which suggests that the beam in the $k_\perp \delta_e = 3.6$ case has more electrons (inspection of the simulation results shows that this is indeed the case). Electrons accelerated from lower original velocities will be more numerous than electrons excited from higher original velocities, since the initial distribution function is Maxwellian.

[49] The total energy flux due to the beam represents a transport of energy away from the pulse. We can compare the size of the beam energy flux at a particular position with the amount of wave Poynting vector entering the simulation box, in order to get an idea of how much energy the wave loses to electrons as it interacts with the plasma. Figure 9 shows the maximum electron energy flux $\max(Q_e)$ in the beam as a function of the magnitude of the wave Poynting vector, $|\mathbf{S}| = |(1/\mu_0)\mathbf{E} \times \mathbf{B}|$, at the top of the simulation box. Since we are interested in the value of $\max(Q_e)$ in the beam, we only compare those simulation runs which created a beam ahead of the pulse. The squares shown in Figure 9 show $|\max(Q_e)|$, calculated at $z = 1\ R_E$, from simulation runs used in the amplitude study (shown in Figure 7a) and the triangles show the same quantity from simulation runs used in the perpendicular scale length study (shown in Figure 8a).

[50] The fraction of the Poynting vector converted into beam electron energy flux is roughly constant for the amplitude study, $\max(Q_e)/|\mathbf{S}| = 0.18$. All of the simulation runs in the amplitude study have $k_\perp \delta_e = 3.6$.

[51] The simulations that are performed with larger perpendicular scale length $k_\perp \delta_e = 3.4$, 2.7 (the two triangles in Figure 9) convert a higher fraction of the wave Poynting vector into electron energy flux. Note that for $k_\perp \delta_e \leq 2.1$ no beam is formed ahead of the pulse. We can see from Figure 8c that as we decrease the perpendicular wave number from $k_\perp \delta_e = 3.6$ to $k_\perp \delta_e = 2.7$, the electrons are accelerated to higher and higher energies, and so this could explain the increase in the fraction of Poynting vector which is taken from the wave. The simulated maximum energy flux in the beam is likely to be an overestimate of the rate of energy transferred from waves to particles, since in our uniform simulations, the wave interacts with the plasma for the entire length of the field line. In particular, it is likely that in a nonuniform magnetic field situation, there will be a preferred location where the plasma has optimum conditions for wave-particle interaction. The fraction of the wave Poynting vector converted to beam energy flux is therefore likely to be less than the estimates reported here.

6. Conclusions

[52] We have used a one-dimensional self-consistent kinetic simulation code to study the response of electrons to shear Alfvén wave pulses. We have reproduced two electron signatures that are commonly observed in low-altitude spacecraft measurements: a velocity-dispersed beam feature and a lower-energy burst of electrons (suprathermal electron burst) that is coincident with the arrival of the pulse. The mechanism which produces velocity-dispersed electron beams is well-known [e.g., *Kletzing*, 1994]. However, the mechanism which produces suprathermal electron bursts is not yet fully established. Our simulation results suggest that suprathermal electron bursts that are accompanied by Alfvénic fluctuations are likely to be due to the local energization of electrons to form the parallel current required to support the wave. This local acceleration and deceleration of the bulk distribution function has been previously reported using linear models by *Kletzing* [1994] and *Kletzing and Hu* [2001]. Here, using a nonlinear self-consistent model, we show how this local energization can manifest itself in differential energy flux and total energy flux, quantities

which are measured by spacecraft and rocket electron instruments. This effect cannot be diagnosed in models which use only test-particles to describe the interaction of electrons with shear Alfvén wave pulses. For example, linear test-particle models [*Thompson and Lysak*, 1996; *Chaston et al.*, 2000; *Su et al.*, 2004] all show resonantly accelerated velocity-dispersed beams of electrons traveling ahead of shear Alfvén wave pulses. However, in order to reproduce a suprathermal electron burst, *Su et al.* [2004] concluded that it was necessary to include a particular oxygen number density profile in their linear gyrofluid/test-particle code. Our results suggest that such specific number density profiles need not be required in order to recreate a suprathermal electron burst-like signature, rather the self-consistent response of the plasma alone may be all that is necessary to explain the burst signature.

[53] We have shown that perturbations in the perpendicular electric field $E_\perp$ associated with shear Alfvén wave pulses are well correlated with enhancements in total parallel electron energy flux Q_e. Enhancements of Q_e which do not occur at the same time as $E_\perp$ perturbations are likely evidence of precipitating electrons in resonantly accelerated beams. Our self-consistent simulation shows that large-amplitude pulses ($q_e\phi \gg k_B T_e$) steepen [*Watt et al.*, 2004] and that electrons in the bulk distribution function are energized by interacting with the antisymmetric $E_\parallel$-field associated with the steepened pulse shape.

[54] We have performed a number of simulations in order to investigate how the amplitude and perpendicular scale length of shear Alfvén wave pulses affects the amount of electron energization. As the shear Alfvén wave pulse amplitude is increased, the magnitude of Q_e measured during the pulse increases. If the perpendicular scale length is such that a beam is formed, then the beam energy increases as the amplitude is increased above a particular threshold (ϕ_0 = 50 V). With the amplitude of the initial pulse held constant, we also investigated the effect of changing the perpendicular scale length of the pulse. The formation of a beam of resonantly accelerated electrons is found to be very sensitive to this parameter. For $k_\perp \delta_e \geq 2.7$ a beam is formed, but for $k_\perp \delta_e \leq 2.1$, no significant beam is observed. We have shown that if the shear Alfvén wave perpendicular scale length and amplitude are such that a beam of precipitating electrons is formed, then typically shear Alfvén wave pulses convert 15–20% of their initial Poynting flux into beam energy flux as they interact with the plasma.

[55] Finally, we have shown that the results from our self-consistent kinetic simulation code can guide the interpretation of electron energy spectra from spacecraft observations. Future developments in the code will provide further understanding of the acceleration of electrons along inhomogeneous geomagnetic field lines.

[56] **Acknowledgments.** CEJW is funded by NSERC and by the Canadian Space Agency. The authors would like to express their gratitude to the FAST science team (C. W. Carlson, P.I.) for use of the EESA, FGM, and electric field data. This work has in part been enabled by the use of WestGrid computing resources, which are funded in part by the Canada Foundation for Innovation, Alberta Innovation and Science, BC Advanced Education, and the participating research institutions.

[57] Shadia Rifai Habbal thanks Craig A. Kletzing and another referee for their assistance in evaluating this paper.

References

Andersson, L., N. Ivchenko, J. H. Clemmons, A. A. Namgaladze, B. Gustavsson, J.-E. Wahlund, L. Eliasson, and R. Y. Yurik (2002), Electron signatures and Alfvén waves, *J. Geophys. Res.*, *107*(A9), 1244, doi:10.1029/2001JA900096.

Arnoldy, R. L., K. A. Lynch, J. B. Austin, and P. M. Kintner (1999), Energy and pitch angle-dispersed auroral electrons suggesting a time-variable, inverted-V potential structure, *J. Geophys Res.*, *104*, 22,613.

Boehm, M. H., C. W. Carlson, J. P. McFadden, and F. S. Mozer (1990), High-resolution sounding rocket observations of large amplitude Alfvén waves, *J. Geophys. Res.*, *95*, 12,157.

Carlson, C. W., R. F. Pfaff, and J. G. Watzin (1998), The Fast Auroral SnapshoT (FAST) mission, *Geophys. Res. Lett.*, *25*, 2013.

Chaston, C. C., C. W. Carlson, R. E. Ergun, and J. P. McFadden (2000), Alfvén waves, density cavities and electron acceleration observed from the FAST spacecraft, *Phys. Scr. T*, *84*, 64.

Chaston, C. C., J. W. Bonnell, L. M. Peticolas, C. W. Carlson, and J. P. McFadden (2002), Driven Alfvén waves and electron acceleration: A FAST case study, *Geophys. Res. Lett.*, *29*(11), 1535, doi:10.1029/2001GL013842.

Chaston, C. C., J. W. Bonnell, C. W. Carlson, J. P. McFadden, R. E. Ergun, and R. J. Strangeway (2003a), Properties of small-scale Alfvén waves and accelerated electrons from FAST, *J. Geophys. Res.*, *108*(A4), 8003, doi:10.1029/2002JA009420.

Chaston, C. C., L. M. Peticolas, J. W. Bonnell, C. W. Carlson, R. E. Ergun, J. P. McFadden, and R. J. Strangeway (2003b), Width and brightness of auroral arcs driven by inertial Alfvén waves, *J. Geophys. Res.*, *108*(A2), 1091, doi:10.1029/2001JA007537.

Clemmons, J. H., M. H. Boehm, G. E. Paschmann, and G. Haerendel (1994), Signatures of energy-time dispersed fluxes measured by Freja, *Geophys. Res. Lett.*, *21*, 1899.

Damiano, P. A., and A. N. Wright (2005), Two-dimensional hybrid MHD-kinetic electron simulations of an Alfvén wave pulse, *J. Geophys. Res.*, *110*, A01201, doi:10.1029/2004JA010603.

Evans, D. S. (1974), Precipitating electron fluxes formed by a magnetic-field aligned potential difference, *J. Geophys. Res.*, *79*, 2853.

Gary, J. B., L. J. Zanetti, B. J. Anderson, T. A. Potemra, J. H. Clemmons, J. D. Winningham, and J. R. Sharber (1998), Identification of auroral oval boundaries from in situ magnetic field measurements, *J. Geophys. Res.*, *103*, 4187.

Goertz, C. K., and R. W. Boswell (1979), Magnetosphere-ionosphere coupling, *J. Geophys. Res.*, *84*, 7239.

Hasegawa, A. (1976), Particle acceleration by MHD surface-wave and formation of aurora, *J. Geophys. Res.*, *81*, 5083.

Hui, C. H., and C. E. Seyler (1992), Electron acceleration by Alfvén waves in the magnetosphere, *J. Geophys. Res.*, *97*, 3953.

Ivchenko, N., G. Marklund, K. Lynch, D. Pietrowski, R. Torbert, F. Primdahl, and A. Ranta (1999), Quasiperiodic oscillations observed at the edge of an auroral arc by Auroral Turbulence 2, *Geophys. Res. Lett.*, *26*, 3365.

Khoyaintsev, Y., N. Ivchenko, K. Stasiewicz, and M. Berthomier (2000), Electron energization by Alfvén waves: Freja and sounding rocket observations, *Phys. Scr. T*, *84*, 151.

Kletzing, C. A. (1994), Electron acceleration by kinetic Alfvén waves, *J. Geophys. Res.*, *99*, 11,095.

Kletzing, C. A., and S. Hu (2001), Alfvén wave generated electron time dispersion, *Geophys. Res. Lett.*, *28*, 693.

Kletzing, C. A., and R. B. Torbert (1994), Electron time dispersion, *J. Geophys. Res.*, *99*, 2159.

Lynch, K. A., D. Pietrowski, R. B. Torbert, N. Ivchenko, G. Marklund, and F. Primdahl (1999), Multiple-point electron measurements in a nightside auroral arc: Auroral Turbulence II particle observations, *Geophys. Res. Lett.*, *26*, 3361.

Lysak, R. L. (1991), Feedback instability of the ionospheric resonant cavity, *J. Geophys. Res.*, *96*, 1553.

Lysak, R. L., and C. W. Carlson (1981), The effect of microscopic turbulence on magnetosphere-ionosphere coupling, *Geophys. Res. Lett.*, *8*, 269.

Mende, S. B., C. W. Carlson, H. U. Frey, T. J. Immel, and J.-C. Gerard (2003), IMAGE FUV and in situ FAST particle observations of substorm aurorae, *J. Geophys. Res.*, *108*(A4), 8010, doi:10.1029/2002JA009413.

Su, Y.-J., R. E. Ergun, W. K. Peterson, T. G. Onsager, R. Pfaff, C. W. Carlson, and R. J. Strangeway (2001), Fast Auroral Snapshot observations of cusp electron and ion structures, *J. Geophys. Res.*, *106*, 25,595.

Su, Y.-J., S. T. Jones, R. E. Ergun, and S. E. Parker (2004), Modeling of field-aligned electron bursts by dispersive Alfvén waves in the dayside auroral region, *J. Geophys. Res.*, *109*, A11201, doi:10.1029/2003JA010344.

Thompson, B. J., and R. L. Lysak (1996), Electron acceleration by inertial Alfvén waves, *J. Geophys. Res.*, *101*, 5359.

Wahlund, J.-E., et al. (1998), Broadband ELF plasma emission during auroral energization: 1. Slow ion acoustic waves, *J. Geophys. Res.*, *103*, 4343.

Watt, C. E. J., R. Rankin, and R. Marchand (2004), Kinetic simulations of electron response to shear Alfvén waves in magnetospheric plasmas, *Phys. Plasmas*, *11*, 1277.

Yamauchi, M., L. Andersson, P.-A. Lindqvist, S. Ohtani, J. H. Clemmons, J.-E. Wahlund, L. Eliasson, and R. Lundin (2001), Acceleration signatures in the dayside boundary layer and the cusp, *Phys. Chem. Earth*, *26*, 195.

I. J. Rae, R. Rankin, and C. E. J. Watt, Department of Physics, University of Alberta, Edmonton, Alberta T6G 2J1, Canada. (cwatt@space.ualberta.ca)

D. M. Wright, Radio and Space Plasma Physics Group, Department of Physics and Astronomy, University of Leicester, University Road, Leicester LE1 7RH, UK.

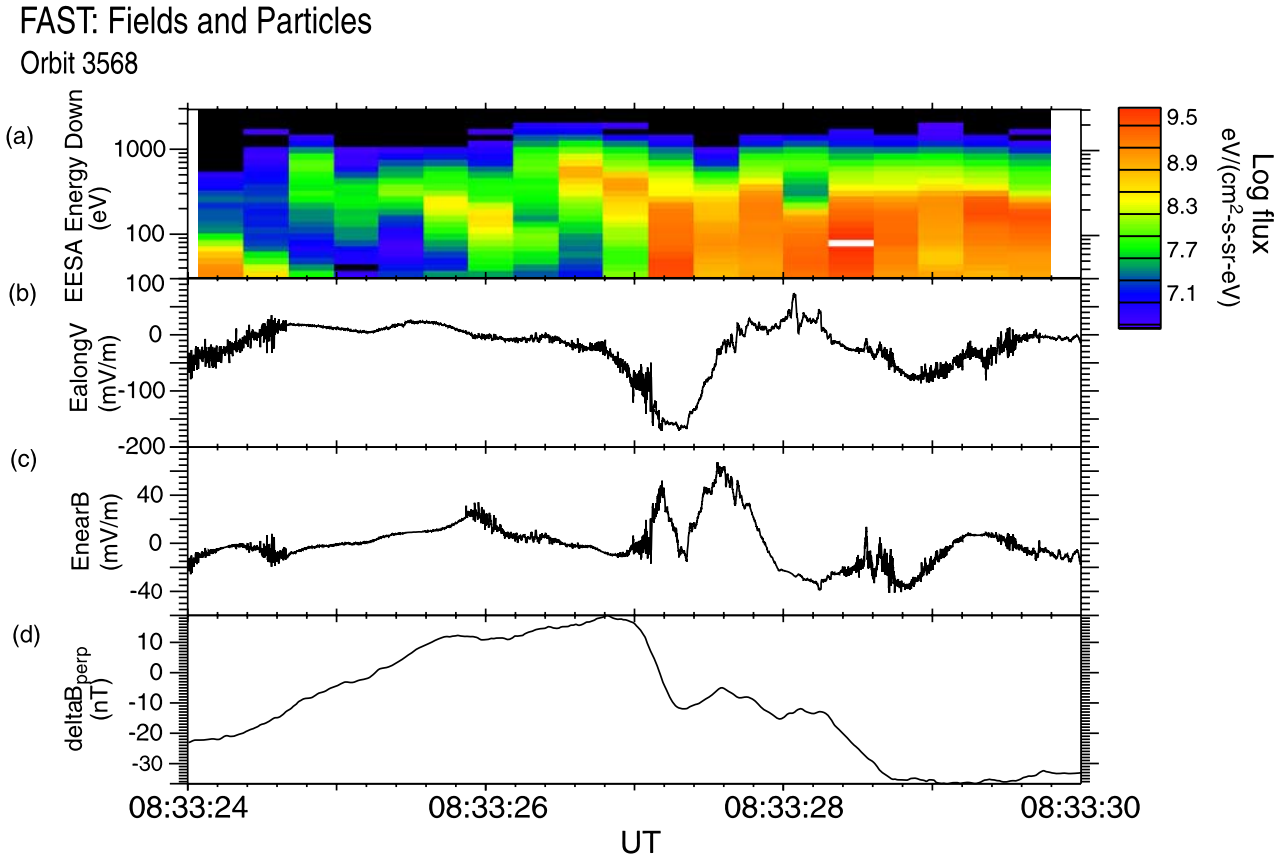

Figure 1. FAST particle and field data from 0833:24UT to 0833:30 UT 17 July 1997 (orbit 3568): (a) Downgoing differential electron energy flux (where electrons are integrated over ±30° from ambient magnetic field direction); (b) Electric field measured along the spacecraft orbit ($E_\perp$); (c) Electric field measured close to the ambient magnetic field direction; (d) Magnetic field measured perpendicular to the ambient magnetic field ($\delta B_\perp$).

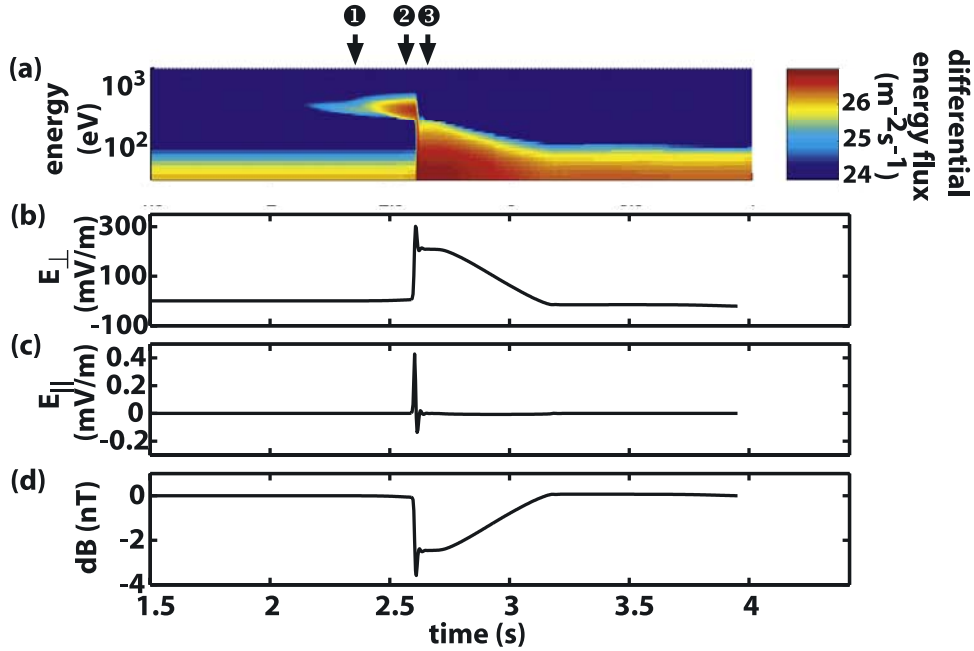

Figure 2. Simulation parameters calculated at $z = 1\ R_E$ from the lower boundary of the simulation as a function of time: (a) Differential energy flux of downgoing electrons; (b) Perpendicular electric field; (c) Parallel electric field; (d) Perpendicular magnetic field. Times marked 1, 2, and 3 are used in Figure 3.

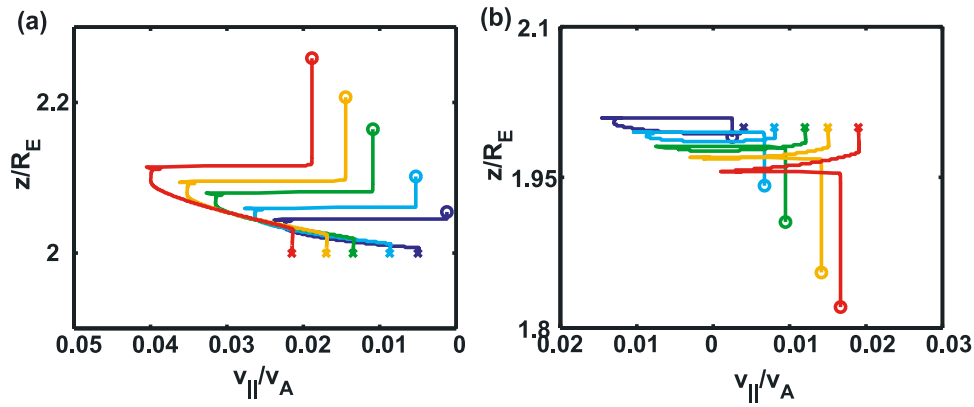

Figure 5. Trajectories of particles traced backwards through the simulation fields from an original position of $z = 2\ R_E$ at $t = 2.6$ s: (a) downgoing and (b) upgoing particles representing the bulk of the heated distribution function.

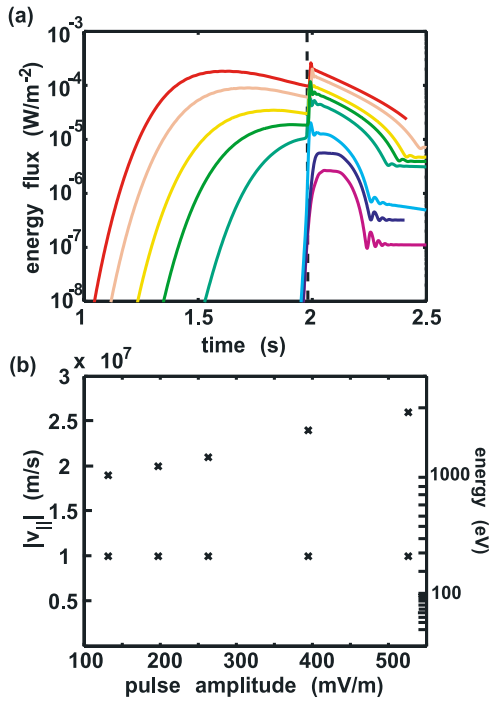

Figure 7. (a) Evolution of the total parallel electron energy flux at $z = 1R_E$ for eight simulation runs with identical initial parameters except for the initial pulse amplitude ϕ_0: from bottom to top ϕ_0 = 5, 10, 20, 50, 75, 100, 150, 200 V. The curves have been lagged such that the arrival of the pulse is synchronized at t = 1.95 s. (b) Velocity range of the resonantly accelerated electrons for those simulation runs which generated a beam (where $\phi_0 \geq 50$ V).